

Novel MMC control for active balancing and minimum ripple current in series-connected battery strings

Damien F. Frost
University of Oxford
17 Parks Road
Oxford, United Kingdom
Phone: +44 (0) 1865-273004
Email: damien.frost@eng.ox.ac.uk
URL: epf.eng.ox.ac.uk

Damien A. Howey
University of Oxford
17 Parks Road
Oxford, United Kingdom
Phone: +44 (0) 1865-273004
Email: david.howey@eng.ox.ac.uk
URL: epf.eng.ox.ac.uk

Abstract—The performance of a string of series-connected batteries is typically restricted by the worst battery cell in the string and a single failure point will render the entire string unusable. To address these issues, we present a decentralised battery management system based on a modular multilevel converter (MMC) with a distributed inductor. This novel MMC design enables each MMC cell to operate autonomously, without central control, by sensing the local inductor voltage. Batteries are loaded with a current proportional to their capacity, and the MMC cells also work together to minimize the output ripple voltage of the full series stack. We show experimentally that the novel decentralized controller implemented in each MMC cell can reduce the output voltage ripple by 69%. We also give an extensive theoretical analysis of the waveforms produced by the MMC using Fourier decomposition. This analysis has applications in all modular multilevel converters.

I. INTRODUCTION

Power electronics is playing a key role in the reduction of greenhouse gas emissions through the integration of green energy technologies with the grid [1],[2]. One area of increased power electronics penetration is electrical energy storage systems such as lithium-ion battery packs [3], where the market is growing very rapidly [4]. Rapid adoption of grid-connected energy storage requires state of the art power electronic converters and energy management systems. Furthermore, since the energy storage device (batteries, for example) is the most expensive component [5], the power electronics should be designed to maximise performance and lifetime whilst ensuring safety [6], [7]. In the worst case scenario, an unmanaged series string of batteries will be limited by the weakest cell [8], thus a single failed cell can render the entire string useless.

In energy storage systems that use electrochemical cells, long term pack performance can be greatly improved by active energy management at the individual cell level, by placing an individual power converter and battery management system on every cell [9], [10]. Recent advancements in wide band gap switching devices, whose cost is expected to decrease over

time, will increase conversion efficiencies (and reduce power losses), and reduce overall system costs through higher power density [11], [12], [13] and decreased cooling requirements [14].

For certain cell chemistries, individual cell monitoring is necessary, and active cell balancing enhances performance. As an example, lithium ion battery technology is unsafe if overcharged, where cells may explode or rupture [15], [16]. Therefore, in order to maximize the energy storage potential of several cells connected in series and in parallel, the state of charge of individual cells in a battery pack must be measured and balanced.

We present work on a cell level battery management system and power converter which uses a decentralized controller strategy to regulate the state of charge of serially connected cells of varying capacities. The distributed battery management system is designed to discharge and charge each cell in a series string of cells proportional to its capacity. The converters are controlled in such a way as to minimize the size of the filtering components in the series string.

II. SYSTEM ARCHITECTURE

An example of the proposed system architecture is shown in Fig. 1. In this example, the system is constructed out of three MMC cells each containing a half bridge switching network similar to the switching networks found in the sub-modules of MMC converters [17]. However each submodule, which we shall in this paper call a ‘smart cell’, has two distinct features that make it different from a standard MMC submodule:

- 1) There exists an independent, autonomous controller in each smart cell.
- 2) Each smart cell includes a small filter inductor, L_{sc} .

The autonomous controllers are used to synchronize the switching events of all of the sub-modules in a string of smart cells to minimize the overall ripple voltage at the output, v_{out} . Each autonomous controller also manages the state of charge (SOC), and monitors the state of health (SOH) of its

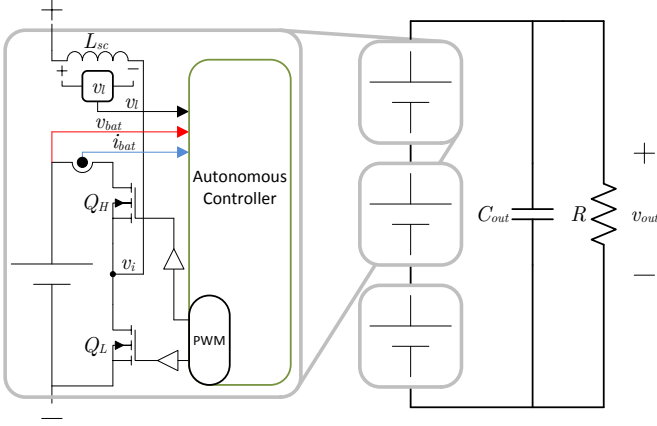


Figure 1: An example of a system containing three ‘smart cells’.

locally connected battery cell. This information is used to apply a duty cycle to the switches Q_L and Q_H , such that the connected battery cell discharges in proportion to its capacity. Discharging all battery cells in proportion to their respective capacities yields two large benefits for the string of smart cells:

- 1) The SOC of all of the battery cells in the string will be synchronized.
- 2) Larger, healthier battery cells will be loaded more than the smaller, more degraded battery cells, thus the pack will degrade at a more uniform rate [18].

The voltage across the small filter inductor L_{sc} is used by the autonomous local controller to determine the optimal switch timings for Q_H and Q_L . Furthermore, by splitting the output filter inductor amongst every smart cell, the inductance is reduced. Eventually L_{sc} could be small enough to be implemented on the trace of a PCB, greatly reducing the cost and size of this component. The dc output load simply requires a filter capacitor, C_{out} .

III. OPTIMAL SWITCHING PATTERN

In order to minimize the output voltage ripple measured at v_{out} an optimal switching pattern of all of the switches Q_H and Q_L must be determined. This is done by all smart cells collectively minimizing the ac rms inductor current. To help solve this problem, a few assumptions will be made about the system of smart cells.

A. Problem and Assumptions

Given set of M battery cells $B_i = \{B_1, B_2, \dots, B_M\}$ with capacities $C_i = \{C_1, C_2, \dots, C_M\}$, our objective is to find a set of phases, $\phi_i = \{\phi_1, \phi_2, \dots, \phi_M\}$ for the turn-on of each smart cell which will minimize the ripple current in local inductor L_{sc} , thus minimize the output ripple voltage.

For simplicity, the nominal voltages of all of the battery cells will be $V_{nom} = V_1 = V_2 = \dots = V_M$, which is a reasonable assumption because the SOC of all of the battery cells will

be synchronized. The duty cycle of each smart cell can be calculated using the following equation:

$$D_i = \frac{C_i}{C_{MAX}} \quad (1)$$

where C_{MAX} is the maximum capacity expected amongst all of the battery cells, or ideally, the maximum value found in the capacity array such that $0 \leq D_i \leq 1$ for all i .

In a series string of smart cells, the voltage applied to each inductor, L_{sc} , will be identical. Thus, we can group all of the distributed inductors together into a single inductor, $L = ML_{sc}$. The voltage across L will be determined by the sum of all of the v_i voltages of the smart cells, and the output dc voltage. The output dc voltage is given by (2):

$$V_{out} = \sum_{i=1}^M D_i V_{nom} = \sum_{i=1}^M \frac{C_i}{C_{MAX}} V_{nom} = \frac{V_{nom}}{C_{MAX}} \sum_{i=1}^M C_i \quad (2)$$

The ac root mean squared (rms) value of the inductor ripple current can be expressed by (3):

$$I_{Lac-rms} = \sqrt{\frac{1}{T_s} \int_0^{T_s} \left[I(s) + \frac{1}{L} \int_s^t (v_{out}(\tau) - V_{out}) d\tau \right]^2 dt} \quad (3)$$

where $I(s)$ is the anti-derivative of $(v_{out}(s) - V_{out})/L$, τ and s are dummy variables of integration, and t is time. The variable $v_{out}(t)$ is defined by (4):

$$v_{out}(t) = \sum_{i=1}^M v_i(t) \quad (4)$$

where $v_i(t)$ is the output voltage of the i^{th} smart cell as measured from the negative terminal of the battery cell to the output terminal of the transistors, as shown in Fig. 1. Therefore, $v_{out}(t)$ is the output voltage of a series string of smart cells.

B. Determine $I_{Lac-rms}$

In order to determine an optimal set of phase angles ϕ_i a function which describes the output of a smart cell in terms of ϕ_i needs to be derived. The output voltage of a smart cell will generally look like a periodic rectangular wave, as shown in Fig. 2.

Using the generalized values in Fig. 2, the Fourier Series representation of the output voltage of any smart cell can be derived, and it is shown in (5) - (9).

$$v_i(t) = d_i(t) V_{nom} \quad (5)$$

$$d_i(t) = \frac{a_{0i}}{2} + \sum_{n=1}^{\infty} \left[a_{ni} \cos\left(\frac{2\pi n t}{T_s}\right) + b_{ni} \sin\left(\frac{2\pi n t}{T_s}\right) \right] \quad (6)$$

where

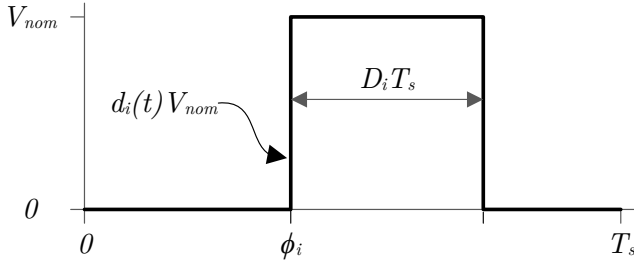


Figure 2: Output voltage, $d_i(t) V_{nom}$, of a smart cell with phase ϕ_i , duty cycle D_i , and switching period, T_s .

$$a_{0i} = 2d_i \quad (7)$$

$$a_{ni} = \frac{1}{n\pi} \left(\sin \left(2\pi n \left(D_i + \frac{\phi_i}{T_s} \right) \right) - \sin \left(2\pi n \frac{\phi_i}{T_s} \right) \right) \quad (8)$$

$$b_{ni} = \frac{1}{n\pi} \left(\cos \left(2\pi n \frac{\phi_i}{T_s} \right) - \cos \left(2\pi n \left(D_i + \frac{\phi_i}{T_s} \right) \right) \right) \quad (9)$$

Now we can substitute (5) into (4) and solve for $I_{Lac-rms}^2$ using (3). It can be shown that the result is:

$$I_{Lac-rms}^2 = \frac{1}{2} \left(\frac{V_{nom} T_s}{2\pi L} \right)^2 \sum_{n=1}^{\infty} \sum_{i=1}^M \sum_{j=1}^M \frac{4}{\pi^2 n^4} \left[\sin(\pi n D_i) \sin(\pi n D_j) \cos \left(\pi n \left(D_i - D_j + 2 \frac{\phi_i}{T_s} - 2 \frac{\phi_j}{T_s} \right) \right) \right] \quad (10)$$

Now let $\theta_x = 2\pi\phi_x/T_s$, so that the switching angles can be measured in radians instead of time:

$$I_{Lac-rms}^2 = \frac{1}{2} \left(\frac{V_{nom} T_s}{2\pi L} \right)^2 \sum_{n=1}^{\infty} \sum_{i=1}^M \sum_{j=1}^M \frac{4}{\pi^2 n^4} [\sin(\pi n D_i) \cdot \sin(\pi n D_j) \cos(\pi n (D_i - D_j) + n(\theta_i - \theta_j))] \quad (11)$$

Equation (11) can now be minimized to determine an optimal set θ_i that will minimize the ac rms current in the inductor L_{sc} , and therefore, the output voltage ripple in v_{out} .

IV. SIMPLIFYING THE PROBLEM

Examining (11), we immediately see that solving for an optimal set θ_i to minimize $I_{Lac-rms}$ is non trivial, and difficult to achieve without significant computational power and global information about the system. Therefore in this section we present a way to identify a set θ_i which will yield a satisfactory solution, with significantly less computational requirements, in a decentralized fashion.

First, let us represent the switching action of the i^{th} smart cell as a vector, v_i , in the unit circle as depicted in Fig. 3. The i^{th} smart cell will turn on at θ_i , and turn off at $\theta_i + 2\pi D_i$. Now define a new vector, v'_i , whose phase places the vector half way between the turn on and turn off times and whose length is $\sin \pi D_i$. Therefore the phase and length of v'_i are given by:

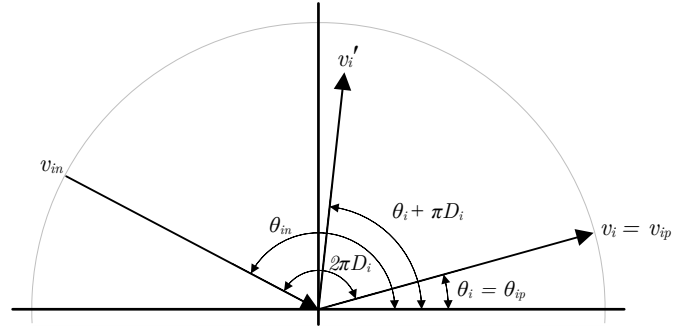


Figure 3: Representing the switching action of the i^{th} smart cell as a vector, with its weighted, phase shifted vector, v'_i . The switching actions of the i^{th} smart cell are also shown as vectors v_{ip} and v_{in} .

$$\angle v'_i = \theta'_i = \theta_i + \pi D_i \quad (12)$$

$$|v'_i| = \sin(\pi D_i) \quad (13)$$

Now apply the transformation described in (12) and (13) to all of the smart cells, and then sum all v'_i , we can find the square of the magnitude of the total sum vector, $|v'_\Sigma|^2$:

$$|v'_\Sigma|^2 = \sum_{i=1}^M \sum_{j=1}^M \sin(\pi D_i) \sin(\pi D_j) \cos(\pi (D_i - D_j) + \theta_i - \theta_j) \quad (14)$$

Equation (14) has the exact same form as (11) when $n = 1$ (i.e. only the fundamental is considered). Therefore, one control algorithm that will yield a good but sub-optimal minimum of (11) is to minimize the magnitude of the total sum vector, $|v'_\Sigma|^2$. This algorithm is used in the simulation study and experimental setup, as presented in the following sections.

V. IMPLEMENTATION OF THE CONTROL ALGORITHM

Calculating the magnitude of the total sum vector using the formula in Equation (14) still requires accurate knowledge of the duty cycles and phase shifts of all of the other smart cells. In order to eliminate communication between smart cells, this approach is still not ideal. This section will address this issue.

A. Smart cell measurements

First, let us consider the measurements a smart cell will be able to make. By measuring the voltage across its local inductor, each smart cell will only know when other smart cells are switching on or off. These switching actions are shown in Fig. 3 as vectors v_{ip} as v_{in} .

Using Fig. 3 as reference, from the point of view of a single smart cell, it will see the switching actions of the i^{th} smart cell as two corresponding voltage transitions: a positive voltage transition across the inductor L_{sc} , depicted by the vector v_{ip} with switching angle θ_{ip} , and its negative corresponding

voltage transition, depicted by the vector v_{in} with switching angle θ_{in} . For a smart cell detecting only one other smart cell, the problem is very trivial and it is easy to determine not only when the other smart cell is switching, but its duty cycle as well.

The challenge arises when multiple smart cells start switching. As soon as a single smart cell needs to determine the switching angles and duty cycles of two or more other smart cells, it is impossible to match every “on” transition with its corresponding “off” transition. We will now show that this is not necessary to yield the optimal solution as defined by (14).

First, use (15) and (16) to replace all of the D_x s and θ_x s with the notation of Fig. 3.

$$\theta_i = \theta_{ip} \quad (15)$$

$$\pi D_i = \left(\frac{\theta_{in} - \theta_{ip}}{2} \right) \quad (16)$$

this yields an expression in terms of measured quantities:

$$|v'_\Sigma|^2 = \sum_{i=1}^M \sum_{j=1}^M \sin\left(\frac{\theta_{in} - \theta_{ip}}{2}\right) \sin\left(\frac{\theta_{jn} - \theta_{jp}}{2}\right) \cdot \cos\left(\left(\frac{\theta_{in} + \theta_{ip}}{2}\right) - \left(\frac{\theta_{jn} + \theta_{jp}}{2}\right)\right) \quad (17)$$

Equation (17) gives the magnitude of the total vector in terms of quantities measured by each smart cell. However, this equation still seems to imply that the “on” transitions must be correctly paired with each of their corresponding “off” transitions. We will now show that this is not the case by first considering the case where only one set of “on” transitions are swapped. Therefore, consider a set of M smart cells, where the k^{th} and l^{th} positive transitions are paired with the l^{th} and k^{th} negative transitions, respectively. It can be shown that:

$$\begin{aligned} |v'_\Sigma|^2 &= \sum_{i=1, i \neq k, i \neq l}^M \sum_{j=1, j \neq k, j \neq l}^M \left[\sin\left(\frac{\theta_{in} - \theta_{ip}}{2}\right) \sin\left(\frac{\theta_{jn} - \theta_{jp}}{2}\right) \right. \\ &\quad \cdot \cos\left(\left(\frac{\theta_{in} + \theta_{ip}}{2}\right) - \left(\frac{\theta_{jn} + \theta_{jp}}{2}\right)\right) \Big] + \sin^2\left(\frac{\theta_{kn} - \theta_{lp}}{2}\right) \\ &\quad + \sin\left(\frac{\theta_{ln} - \theta_{kp}}{2}\right) \sin\left(\frac{\theta_{kn} - \theta_{lp}}{2}\right) \cos\left(\left(\frac{\theta_{ln} + \theta_{kp}}{2}\right) - \left(\frac{\theta_{kn} + \theta_{lp}}{2}\right)\right) \\ &\quad + \sin^2\left(\frac{\theta_{ln} - \theta_{kp}}{2}\right) + \sin\left(\frac{\theta_{ln} - \theta_{kp}}{2}\right) \\ &\quad \cdot \sin\left(\frac{\theta_{ln} - \theta_{kp}}{2}\right) \cos\left(\left(\frac{\theta_{kn} + \theta_{lp}}{2}\right) - \left(\frac{\theta_{ln} + \theta_{kp}}{2}\right)\right) = \\ &\quad \sum_{i=1}^M \sum_{j=1}^M \sin\left(\frac{\theta_{in} - \theta_{ip}}{2}\right) \sin\left(\frac{\theta_{jn} - \theta_{jp}}{2}\right) \cos\left(\left(\frac{\theta_{in} + \theta_{ip}}{2}\right) - \left(\frac{\theta_{jn} + \theta_{jp}}{2}\right)\right) \end{aligned} \quad (18)$$

By extension, we can swap any pair and any number of transitions with each other and get the same result. Therefore,

in order to minimize the total sum vector of (14), each smart cell need only know when the positive and negative transitions *occur* to determine its local optimal switching pattern. Moreover, it can be shown that these results are also true for all harmonics, 1 to n .

B. Controller Design

A MATLAB-Simulink model of a smart cell using the theory developed in this work was built using the SimPower-Systems toolbox. The model uses the Simscape battery model and MOSFETs to simulate the power circuit. The controller was implemented as an embedded MATLAB function, and is executed once per switching cycle when the upper MOSFET, Q_H , is switched on.

Figure 4 illustrates the algorithm the controller implements as a block diagram. Steps 1 through 8 outlined in green are the steps implemented by the embedded MATLAB function.

- 1) **Edge Detector:** Detects all of the positive and negative transitions that occur during every switching cycle, T_s . The edge detector handles cases where multiple smart cells turn on or off at the same time by tracking the different voltage levels measured with v_l .
- 2) **Transformation:** The positive and negative edges are paired together to form a set of sensed smart cells. The transformation described by (12) and (13) is applied.
- 3) **Sum all vectors:** All of the vectors found and transformed are added together as described by (14)
- 4) **Subtract local v'_0 :** The vector which describes the switching action of the local cell is subtracted from the total sum vector to yield v'_{other} .
- 5) **Calculate reference:** In order to minimize the sum of the total vector, $\angle v'_{ref}$ is calculated by simply adding π to $\angle v'_{other}$. In this way, the total sum vector is minimized.
- 6) **Calculate angle:** The actual phase shift of the local smart cell is calculated by reversing the transform of (12).
- 7) **Apply limits:** $\pm 2\pi$ is added to $\angle v_{ref}$ until it lies between $-\pi$ and π .
- 8) **Calculate phase:** Finally, the phase that will be sent to the PWM generator is calculated by multiplying the phase error ($0 - \angle v_{ref}$) by the duty cycle of the local smart cell, D_0 , and a gain of G_{PhCtrl} . By multiplying the error by the duty cycle, the phase shifts of smart cells with different capacities will change at different rates, allowing the system to find an equilibrium point.
- 9) **PWM Generator:** θ_0^{new} is used by the PWM generator to produce gating signals for the MOSFETs.

VI. SIMULATION STUDY

A simulation study of a series string of three smart cells was undertaken. Fig. 1 shows a schematic of the 3 smart cell pack. Table I lists the simulation parameters used.

The simulation consists of the three smart cells operating completely independently of each other. The optimal switching controller is turned on 1.0 ms into the simulation. A value of $C_{MAX} = 4.00$ Ah was pre-programmed into each smart cell.

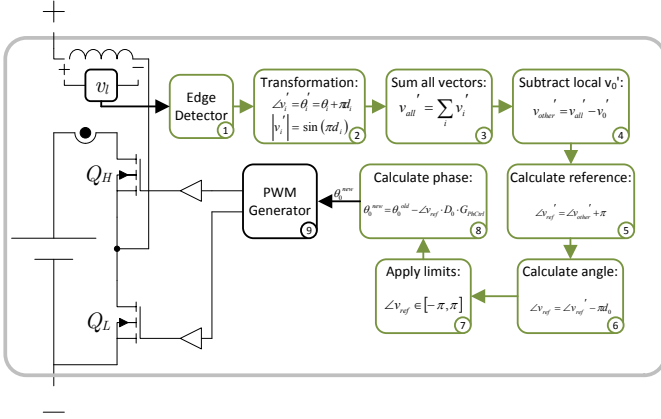


Figure 4: Control block diagram of a smart cell built in MATLAB-Simulink. The blocks outlined in green are implemented in an embedded MATLAB function.

Table I: Parameters of the three smart cell simulation study.

Description	Parameter	Value
Battery Cell Capacities	C_1	0.75 Ah
	C_2	1.20 Ah
	C_3	3.00 Ah
Smart Cell Parameters	L_{sc}	100 μH
	f_s	50 kHz
	V_{nom}	4.19 V
Output	C_{out}	4.7 μF
	R	23.5 Ω

Fig. 5 shows how different characteristics of the system evolve over the length of the simulation. The smart cells initially all turn on at the same time, which produces a very high ac rms ripple current in the inductor, as shown in the inset graphs. At the beginning of the simulation, $I_{Lac-rms}$ is 34 mA rms, and the peak-to-peak output voltage, v_{out-pp} , is 64 mV. After the optimal switching controller is engaged, the phase shift of each smart cell gradually evolves smoothly into its steady state value. At the end of the simulation, $I_{Lac-rms}$ and v_{out-pp} have improved considerably to 10 mA rms and 11 mV, respectively.

VII. EXPERIMENTAL RESULTS

The theory developed in this work was tested in the laboratory with an experimental setup consisting of three smart cells in series, as shown in Fig. 1 using the parameters listed in Table I. The hardware was built around ARM's *mbed* platform, where each smart cell is implemented with the NUCLEO-F401RE board and a custom printed circuit board (PCB) containing the power stage. They were tested using laboratory power supplies. Fig. 6 shows a photograph of the three smart cells built in the laboratory.

The NUCLEO-F401RE board was chosen for its relatively powerful micro-controller, the STM32F401RET6, in order

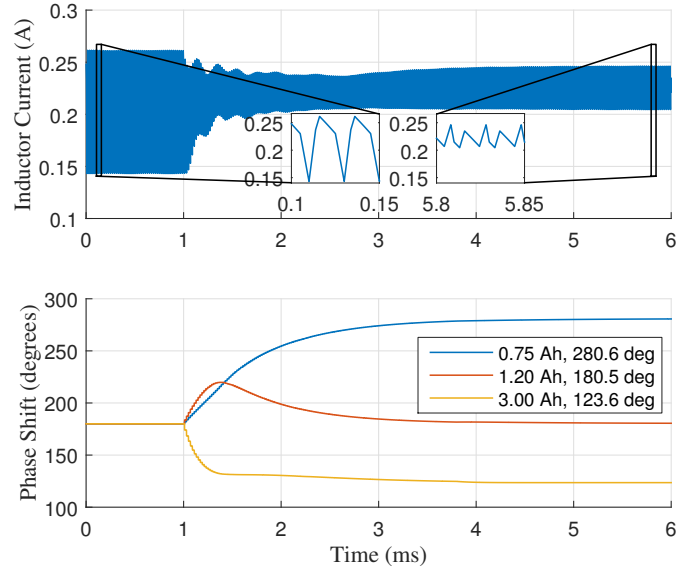


Figure 5: Summary of the simulation results of a three smart cell pack. The smart cell controllers are turned on at 1.0 ms. The ac rms current in the inductor is improved from 34 mA rms to 10 mA rms. Although not shown, the peak-to-peak ripple voltage on the capacitor is improved from 64 mV to 11 mV.

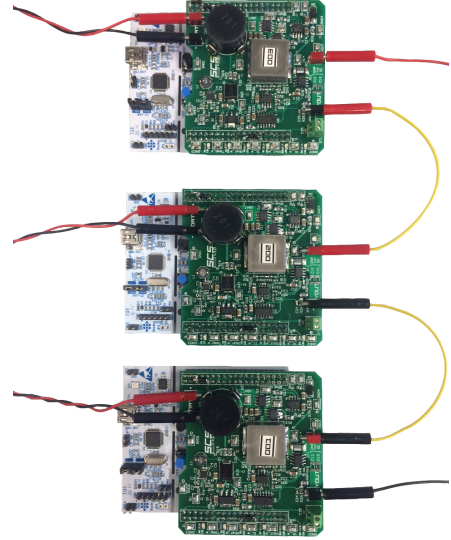


Figure 6: A photograph of the three smart cells tested in the laboratory. The battery cell connections are on the left, and the output is on the right. The smart cells were connected to laboratory power supplies for the tests.

to focus attention on how the smart cell controller can be implemented in hardware. The STM32F401RET6 is based on the ARM 32-bit Cortex-M4 CPU and has a floating point unit.

Fig. 7 shows an oscilloscope screen shot of the three smart cells operating and finding their optimal switching pattern.

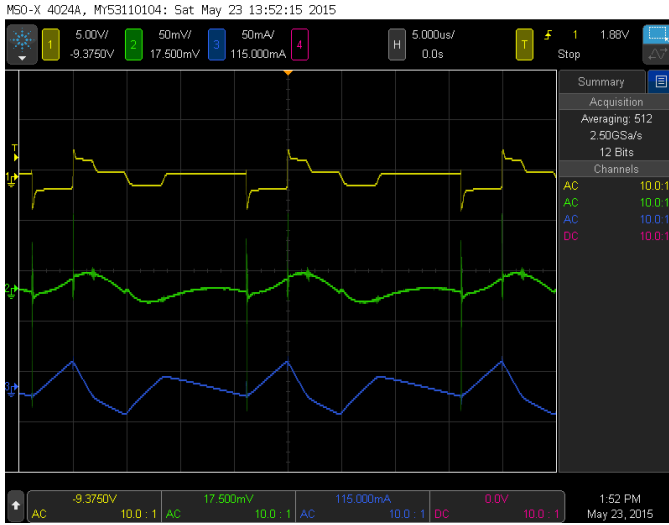


Figure 7: An oscilloscope screen shot of the three smart cells operating at their optimal switching pattern, averaging applied with 512 samples. Channel 1, top yellow, is the voltage across L_{sc} of the first smart cell with a capacity of C_1 . Channel 2, middle green, is the output voltage ripple. Channel 3, bottom blue, is the current in the smart cell inductors.

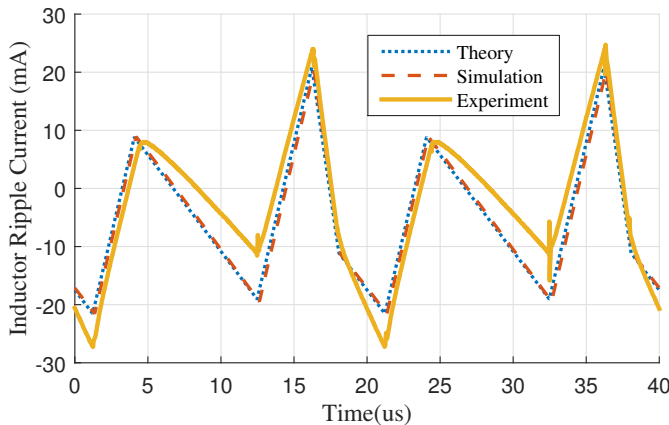


Figure 8: L_{sc} currents from the theoretical analysis, simulation and experiment.

Using the data from the oscilloscope, we can plot the measured L_{sc} current along with the theoretical and simulated L_{sc} currents, and this is shown in Fig. 8. The experimental L_{sc} current matches very well with the theoretical and simulated values, and is well within experimental error when the variation of the inductance of each L_{sc} is taken into account, which is $\pm 20\%$ for the Vishay Dale IHLP6767GZER101M11 inductor used in these experiments.

The peak-to-peak voltage ripple from the experiments was reduced to 24 mV from 78 mV and the peak-to-peak L_{sc} current ripple was reduced to 54 mA from 102 mA.

CONCLUSIONS AND FUTURE WORK

The energy management of series-connected battery cells was addressed with a novel decentralised battery management system based on an MMC topology. Each MMC submodule, or smart cell, operates autonomously within a string to minimize the output ripple voltage and balance the batteries. A smart cell contains a completely decentralized controller, and a small inductor, L_{sc} , used to sense transitions in the rest of the string. We developed a theoretical approach to minimising the output voltage ripple by deriving an equation for the ac rms ripple current in the smart cell inductors using Fourier decomposition, taking as inputs the duty cycle and switching phase of each smart cell and minimising this. This result can be applied to MMC converters in general. In order to simplify the approach so that it can be locally applied in a set of autonomous smart cell controllers we also derived a solution that yields near-optimal results by minimising the magnitude of the total sum vector of all smart cell voltages. This is equivalent to only considering the fundamental of the Fourier series of each switching waveform. The theory was demonstrated in simulation and experimental results, where a system of three smart cells were able to find a stable operating point, and the output voltage ripple was reduced from 78 mV to 24 mV.

ACKNOWLEDGMENT

The authors acknowledge the financial support provided by Newtons4th Ltd. (N4L), the Natural Sciences and Engineering Research Council of Canada (NSERC) and Jesus College Oxford. This work also benefited from equipment funded by the John Fell Oxford University Press (OUP) Research Fund and an EPSRC Capital Grant (ref. EP/J021199/1).

REFERENCES

- [1] B. Bose, "Global warming: Energy, environmental pollution, and the impact of power electronics," *Industrial Electronics Magazine, IEEE*, vol. 4, no. 1, pp. 6–17, March 2010.
- [2] —, "Power electronics and motor drives recent progress and perspective," *Industrial Electronics, IEEE Transactions on*, vol. 56, no. 2, pp. 581–588, Feb 2009.
- [3] S. Vazquez, S. Lukic, E. Galvan, L. Franquelo, and J. Carrasco, "Energy storage systems for transport and grid applications," *Industrial Electronics, IEEE Transactions on*, vol. 57, no. 12, pp. 3881–3895, Dec 2010.
- [4] S. Wilkinson. The grid-connected energy storage market is set to explode, reaching a total of over 40 gw of installations by 2022. IHS Technology. [Online]. Available: <https://technology.ihs.com/483008/the-grid-connected-energy-storage-market-is-set-to-explode-reaching-a-total-of-over-40-gw-of-installations-by-2022>
- [5] H. Chen, T. N. Cong, W. Yang, C. Tan, Y. Li, and Y. Ding, "Progress in electrical energy storage system: A critical review," *Progress in Natural Science*, vol. 19, no. 3, pp. 291 – 312, 2009. [Online]. Available: <http://www.sciencedirect.com/science/article/pii/S100200710800381X>
- [6] D. Andrea, *Battery Management Systems for Large Lithium-Ion Battery Packs*. Artech House Publishers, October 2010.
- [7] J. Kimball, B. Kuhn, and P. Krein, "Increased performance of battery packs by active equalization," in *Vehicle Power and Propulsion Conference, 2007. VPPC 2007. IEEE*, Sept 2007, pp. 323–327.
- [8] J. Zhang, S. Ci, H. Sharif, and M. Alahmad, "Modeling discharge behavior of multicell battery," *Energy Conversion, IEEE Transactions on*, vol. 25, no. 4, pp. 1133–1141, Dec 2010.
- [9] P. Weicker, *A Systems Approach to Lithium-Ion Battery Management*. Artech House Publishers, October 2013.

- [10] C. Birkel, D. Frost, A. Bizeray, R. Richardson, and D. Howey, "Modular converter system for low-cost off-grid energy storage using second life li-ion batteries," in *Global Humanitarian Technology Conference (GHTC), 2014 IEEE*, Oct 2014.
- [11] M. Rodriguez, Y. Zhang, and D. Maksimovic, "High-frequency pwm buck converters using gan-on-sic hemts," *Power Electronics, IEEE Transactions on*, vol. 29, no. 5, pp. 2462–2473, May 2014.
- [12] D. Reusch, D. Gilham, Y. Su, and F. Lee, "Gallium nitride based 3d integrated non-isolated point of load module," in *Applied Power Electronics Conference and Exposition (APEC), 2012 Twenty-Seventh Annual IEEE*, Feb 2012, pp. 38–45.
- [13] T. McDonald and V. President, "Gan based power technology stimulates revolution in conversion electronics," *Electronics in Motion and Conversion*, pp. 2–4, 2009.
- [14] J. Millan, P. Godignon, X. Perpina, A. Perez-Tomas, and J. Rebollo, "A survey of wide bandgap power semiconductor devices," *Power Electronics, IEEE Transactions on*, vol. 29, no. 5, pp. 2155–2163, May 2014.
- [15] R. A. Leising, M. J. Palazzo, E. S. Takeuchi, and K. J. Takeuchi, "Abuse testing of lithium-ion batteries: Characterization of the overcharge reaction of licoo2/graphite cells," *Journal of The Electrochemical Society*, vol. 148, no. 8, pp. A838–A844, 2001.
- [16] L. Lu, X. Han, J. Li, J. Hua, and M. Ouyang, "A review on the key issues for lithium-ion battery management in electric vehicles," *Journal of Power Sources*, vol. 226, no. 0, pp. 272 – 288, 2013. [Online]. Available: <http://www.sciencedirect.com/science/article/pii/S0378775312016163>
- [17] A. Lesnicar and R. Marquardt, "An innovative modular multilevel converter topology suitable for a wide power range," in *Power Tech Conference Proceedings, 2003 IEEE Bologna*, vol. 3, June 2003, pp. 6 pp. Vol.3–.
- [18] S. S. Choi and H. S. Lim, "Factors that affect cycle-life and possible degradation mechanisms of a li-ion cell based on licoo2," *Journal of Power Sources*, vol. 111, no. 1, pp. 130 – 136, 2002. [Online]. Available: <http://www.sciencedirect.com/science/article/pii/S0378775302003051>